Allosteric Cross Talk between Cadherin Extracellular Domains

Quanming Shi,[†△] Venkat Maruthamuthu,[†△] Fang Li,[‡] and Deborah Leckband[†§¶*]
[†]Department of Chemical and Biomolecular Engineering, [‡]Department of Mechanical Science and Engineering, [§]Department of Biochemistry, and [¶]Department of Chemistry, University of Illinois at Urbana-Champaign, Urbana, Illinois

ABSTRACT Atomic force microscopy and surface force apparatus measurements determined the functional impact of the cadherin point mutation W2A and domain deletion mutations on C-cadherin binding signatures. Direct comparison of results obtained using both experimental approaches demonstrates that C-cadherin ectodomains form multiple independent bonds that require different structural regions. The results presented reveal significant interdomain cross talk. They further demonstrate that the mutation W2A not only abolishes adhesion between N-terminal domains, but allosterically modulates other binding states that require functional domains distal to the N-terminal binding site. Such allosteric effects may play a prominent role in modulating adhesion by Type I classic cadherins, cadherin oligomerization at junctional contacts, and propagation of binding information to the cytoplasmic region.

INTRODUCTION

Cadherins are a superfamily of calcium-dependent cell surface proteins. The classic cadherins are the principal group of proteins mediating intercellular adhesion and the most extensively studied members of the cadherin superfamily. Type I classic cadherins are Ca^{2+}-dependent adhesion proteins that are expressed in almost all solid tissues (1). They are required for morphogenesis and the organized regulation of mature tissues (2), and cadherin dysfunction is linked to tumor malignancy (3).

Classic cadherins comprise an extracellular region that folds into five structurally homologous β-barrel domains, a transmembrane segment, and a cytoplasmic domain. The sequence homology among Type I classic cadherins, in particular, implies that determining basic molecular mechanisms of cadherin adhesion and its regulation would contribute to the understanding of a range of critical biological processes involving cadherins such as cell sorting during morphogenesis or the regulation of tissue barriers (2).

Crystal structures and mutagenesis studies (4,5) support a model in which the tryptophan at position 2 (W2) on the first extracellular domain (EC1) docks in a conserved hydrophobic pocket of the same molecule or an opposing cadherin (6,7). The hypothesis that the mutual exchange of W2 between opposing cadherins mediates adhesion is supported by immunoprecipitation (8,9), cross-linking (4,10,11), electron microscopy (7), NMR (6), and x-ray crystallographic (12,13) data.

There is also evidence that cadherins form bonds that do not involve W2 docking. It is postulated that in addition to adhesive bonds between cells, cadherins form lateral dimers on the cell surface (14,15). Studies show that W2A mutants have residual binding activity, as demonstrated in bead aggregation assays (16,17) and biophysical measurements (18). W2A mutants also accumulate at cell-cell contacts (4,5). Biophysical studies reported by different laboratories (19–26) demonstrate that reconstitution of the adhesive properties of wild-type cadherin requires domains in addition to the N-terminal extracellular domain 1, EC1. The initial cadherin-mediated cell-binding kinetics exhibits distinct signatures that require both EC1 and EC3 (21). These results argue for additional cadherin interactions that utilize domains other than EC1.

Recent findings also suggest that allosteric cross talk between EC domains regulates cadherin function. Point mutations in calcium-binding sites distal to EC1 at the EC1/EC2 and EC2/EC3 junctions nearly abolish EC1-mediated adhesion (17,27). E-cadherin point mutations associated with familial gastric cancer are distributed along the entire ectodomain, and are associated with adhesion and localization defects (28,29). Allostery is often implicated in the regulation of protein function (30). In mechanochemical transduction, adhesion receptors convert mechanical signals into biochemical reactions, as exemplified by integrins (31). Although the EC regions of classic cadherins are relatively rigid and do not undergo large conformational changes as integrins do (31), findings suggest long-range allosteric communication between cadherin EC domains (16,17,32). Molecular dynamics simulations (33) also suggest that calcium binding at the EC1/EC2 junction affects W2 docking to the hydrophobic pocket. However, determining how this interdomain cross talk impinges on cadherin function requires quantitative approaches capable of interrogating the role of both W2 and EC domains in cadherin binding.

This work describes surface force apparatus (SFA) measurements and complementary single-molecule atomic force microscopy (AFM) measurements with the W2A point mutant and with domain deletion mutants of *Xenopus* cleavage-stage C-cadherin. Both approaches detected multiple

Submitted December 4, 2009, and accepted for publication March 31, 2010.

△Quanming Shi and Venkat Maruthamuthu contributed equally to this work.

*Correspondence: Leckband@illinois.edu

Editor: Peter Hinterdorfer.

0006-3495/10/07/0095/10 $2.00

doi: 10.1016/j.bpj.2010.03.062

binding interactions between cadherin ectodomains that map to different structural domains. This study compares extensive structure/function analyses of single bond rupture measurements with SFA measurements. We show that biochemical perturbations cause distinct changes in the force signatures. These complementary studies confirm that cadherin ectodomains form multiple, uncorrelated bound states, and further reveal cooperativity between EC domains. They also provide quantitative evidence for allosteric interactions between the W2 binding pocket and distal functional domains. These findings suggest a more comprehensive binding mechanism in which N-terminal domains both mediate cadherin adhesion and modulate other functional interactions between Type I classic cadherin ectodomains.

MATERIALS AND METHODS

Chemicals

1,2-Dipalmitoyl-*sn*-glycero-3-phosphoethanolamine (DPPE) was obtained from Avanti Polar Lipids (Alabaster, AL). 6-(9-(2,3-Bis(dodecyloxy) propyl])3,6,9- trioxanonyl-1-oxycarboxylamino)-2-(di(carboxymethyl)amino) hexanoic acid (NTA-TRIG-DLGE) was custom-synthesized by Neuftech Chemicals (Vancouver, BC, Canada). 1,8-octanedithiol, 6-mercapto-1-hexanol, dodecanethiol, and tris base were from Sigma (St. Louis, MO), all high purity salts were from Aldrich (St. Louis, MO), and poly(ethyleneglycol)-α-maleimide, ω-N-hydroxysuccinimide ester (NHS-PEG-MAL, 3400 Da) was purchased from Nektar Therapeutics (Huntsville, AL).

Protein expression and purification

Chinese hamster ovary (CHO) cells were engineered to secrete the suitably tagged fragments of C-cadherin ectodomains. The proteins were modified at their C-termini with either a human Fc domain or a hexahistidine tag. The hexahistidine-tagged proteins included the wild-type C-cadherin EC domains 1–5 (CEC1–5-His_6) and the W2A C-cadherin mutant W2A-His_6. The Fc-tagged proteins included CEC1–5 and the C-cadherin domain deletion fragments CEC12, CEC1245, CEC1–3, CEC1–4, and CEC345. Stable CHO cell lines expressing these soluble proteins were a gift from Prof. B. Gumbiner (University of Virginia, Charlottesville, VA). The expression and purification of both the His_6-tagged and Fc-tagged proteins is described elsewhere (24,31). Protein purity was assessed by sodium dodecyl sulfate polyacrylamide gel electrophoresis and by Western blot analysis.

Determination of cadherin densities on supported bilayers used in SFA measurements

The surface density (number/μm^2) of immobilized proteins used for SFA measurements was determined by surface plasmon resonance (SPR) (34). Samples were prepared for SPR measurements as follows. The proteins were immobilized on an NTA-TRIG-DLGE monolayer, which was supported on an alkanethiol monolayer self-assembled on a thin gold film on glass. The 390-Å gold layer was thermally evaporated onto a 10-Å chromium adhesion layer on glass slides (Corning, Corning, NY). The slides were initially cleaned with a 1:1:1 $H_2O/HCl/H_2O_2$ mixture, rinsed copiously with ultrapure water, and then dried under a stream of nitrogen. The gold-coated slides were then incubated in an ethanolic solution of 0.5 mM dodecanethiol to form a self-assembled monolayer (SAM). The NTA-TRIG-DLGE monolayer was then deposited on the SAM by Langmuir-Blodgett deposition from a subphase containing buffer A (20 mM Tris, 50 mM $NaNO_3$, 2 mM $Ca(NO_3)_2$, and 50 μM $NiSO_4$, pH 7.5) at room temperature. The deposition was at a constant surface pressure of 34 mN/m (65 $Å^2$/lipid).

Histidine-tagged cadherin ectodomains were immobilized directly to the NTA-TRIG-DLGE monolayer by incubating bilayers with 1-μM protein solutions for 1 h at room temperature. Fc-tagged proteins were bound to an immobilized hexahistidine fragment of protein A, which was prepared by incubating a 5-μM solution of an engineered protein A fragment with the NTA-TRIG-DLGE monolayer in buffer A for 1 h at room temperature. The Fc-tagged proteins (0.1 μM) were then incubated with the protein A layer for 2 h at room temperature.

The surface densities of immobilized cadherin ectodomain fragments were quantified with a home-built SPR instrument. A Teflon SPR cell maintains the sample under buffer. Protein densities were determined from the change in the plasmon resonance angle from before to after protein adsorption, and use of analysis software from R. Corn (University of California, Irvine, CA). The protein density was determined using the measured thickness of the immobilized cadherin layer and a protein refractive index of 1.44. The thickness included the combined thickness of the Fc domain and protein A, when relevant.

Sample preparation for SFA measurements

In the SFA measurements, oriented cadherin monolayers were immobilized on planar bilayers supported on freshly cleaved mica sheets. The mica sheets were coated on one side with a thermally evaporated 400- to 500-Å silver film. The mica sheets were then glued silvered-side down onto hemicylindrical silica lenses. A monolayer of DPPE was deposited on the mica by Langmuir-Blodgett deposition from a water subphase at room temperature and a constant surface pressure of 37 mN/m (43 $Å^2$/lipid). An outer layer of NTA-TRIG-DLGE was then deposited onto the DPPE layer as described above for the SPR samples.

Proteins were immobilized on the supported bilayers as described for the SPR samples. The protein incubation was performed in a custom-made sample holder inside a beaker with an incubation volume of 1 ml. The surfaces were then rinsed with buffer, and the samples (Fig. 1 *A*) were assembled in the SFA while submerged in buffer.

SFA setup, calibration, and measurements

The SFA quantifies the force between two macroscopic curved surfaces as a function of their separation distance (35). The proteins immobilized on supported bilayers are supported on mica sheets (Fig. 1 *A*). The upper disc is mounted on a piezo tube, with an extension/voltage characteristic of ~7 Å/V, and voltage applied to the piezo tube controls the disc separation. The absolute surface separation is measured within ± 1 Å by multiple-beam interferometry (36). To define the separation between the bilayers, we first measured the wavelengths of the interference fringes at contact between the DPPE monolayers in air (defined as $T = 0$; Fig. 1 *A*). After depositing the outer NTA-DLGE layer, the distance of closest intersurface approach, relative to DPPE contact in air, increases by $2 \times T_{NTA\text{-}DLGE}$. The absolute bilayer separation is then $D = T - 2 \times T_{NTA\text{-}DLGE}$.

In the Mark II SFA used for these studies, the bottom silica disc is mounted on a leaf spring with a spring constant of 156 N/m, and the total force between the discs is obtained from the spring deflection and Hooke's Law. The SFA measurements quantify the normalized force, F_c/R, between the two curved surfaces as a function of D. The normalized force between two curved surfaces is related to the energy between equivalent flat surfaces, E_f, by the Derjaguin approximation (37), $F_c = 2\pi R E_f$. Here R is the geometric mean of the radii of curvature of crossed cylindrical lenses, $R = \sqrt{R_1 R_2}$. Thus, F_c/R is proportional to the interaction energy between equivalent planar surfaces. The uncertainty in the normalized force is $\Delta F/R = \pm 0.1$ mN/m (mJ/m^2).

The adhesion energy/area is related to the pull-off force, F_{po}, by the Johnson-Kendall-Roberts theory, $E_a = 2F_{po}/3\pi R$ (37). The minima in the

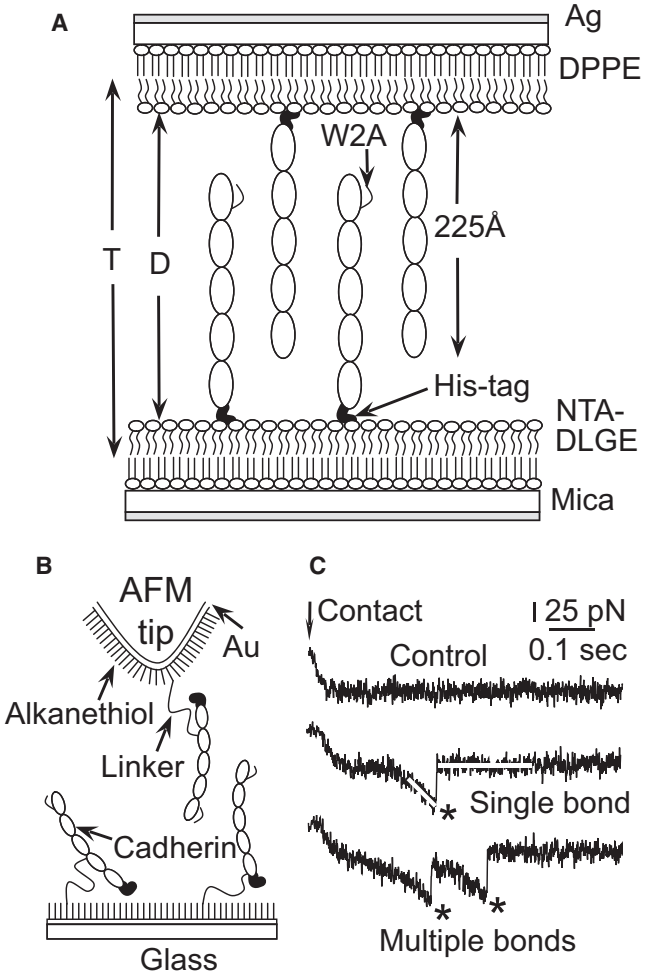

FIGURE 1 (*A*) Schematic of sample configurations used in SFA measurements. Cadherins are immobilized on supported lipid bilayers. D, interbilayer distance; T, distance between DPPE monolayers. Here, CEC1–5-His_6 is immobilized on the upper membrane and W2A-His_6 on the lower membrane. (*B*) Schematic of sample configuration in AFM measurements. The proteins are covalently bound to SAMs on the tip and glass slide via 3400-mol wt PEG linkers. (*C*) Typical force-extension curves measured with the AFM at $r_F = 400$ nm/s, showing contact (*arrow*) followed by either no binding (*top*) or formation of a single bond (*middle trace*) and multiple bonds (*bottom*) upon tip retraction. The solid line in the middle trace of *C* shows the linear fit to the force-extension curve just before bond rupture (*asterisk*). The slope of this line is used to determine the pulling rate just before bond rupture.

force-distance curves occur at the minima in the potential between parallel planar surfaces. In these studies, the pull-off positions, together with cadherin domain deletion mutants, were used to identify structural segments mediating cadherin adhesion (26,38). From the adhesion energy/area and the protein coverage, Γ (molecules/unit area), the estimated average bond energy, E_b, is $E_f = \Gamma(E_b/[1 + \exp(-E_b/k_BT)])$.

All force curves were measured at least 10 times and from at least two different regions of the sample surface ($N > 20$). We also conducted >12 measurements each for CEC1–5/CEC1–5, W2A/W2A, and W2A/CEC1–5 interactions. The reproducibility of successive measurements at identical contact regions indicates that adhesive failure occurs at protein-protein bonds and does not involve lipid pull-out or protein detachment from the membranes (39).

Sample preparation for AFM measurements

Cadherins were covalently bound directly to the AFM tip and substrates, as described previously (40,41) (Fig. 1 *B*). Glass slides and Si_3N_4 cantilevers (Veeco Probes, Camarillo, CA) were cleaned, then coated with a gold film. SAMs of a mixture of 1,8-octanedithiol and 6-mercapto-1-hexanol were self-assembled on the gold film. The ratio of the two alkanethiols was adjusted empirically to achieve a protein density that would generate sufficiently low binding probabilities (10–20%). This ensured that the rupture events reflected single bonds. The monolayers were then reacted with an aqueous solution of 1 mg/ml NHS-PEG-MAL for 15 min at room temperature. After rinsing, proteins were immobilized to the terminal NHS groups by incubation at 0.06 mg/ml in 20 mM HEPES, 100 mM NaCl, 2 mM $CaCl_2$, pH 7.5, for 1 h.

AFM measurements of single bond rupture

Cadherin bond rupture measurements were done with a MFP 1-D instrument (Asylum Research, Santa Barbara, CA) controlled with Igor Pro software (WaveMetrics, Lake Oswego, OR), as described (40). The optical lever sensitivity was first calibrated by pressing the tip against a hard surface to obtain the tip deflection in nanometers. The cantilever spring constants, calibrated using the thermal method (42), were 0.01–0.025 N/m. In a typical measurement, the tip was moved to the surface until the impingement force reached ~30 pN, and was then retracted at constant velocity. For every protein combination, the surface densities of the protein on the tip and on the surface were such that <10–20% of these force curves recorded a binding event ($p > 0.9$). This increases the likelihood that the binding involves a single-molecule event (43). Controls performed with 5 mM EDTA inactivated cadherin and reduced the binding frequency to <3% of tip-surface contacts.

Fig. 1 *C* shows typical force-extension curves obtained for the cases of no adhesion, single bond rupture, and multiple bond rupture at a pulling rate of 400 nm/s. The occurrence of multiple bond rupture events was minimized by lowering the overall binding frequency. Traces exhibiting multiple rupture events were not analyzed further. The effective pulling rate is determined from the slope of the curve just before bond rupture. This corresponds to the elastic stretch of the polymer linker, and the slope gives the effective pulling rate. From ~2000 force curves, those corresponding to the average effective pulling rate within $\pm 20\%$ are used to generate histograms of the rupture force distributions.

The rupture force data were analyzed according to Evans and Ritchie (44). For a bond confined by a single barrier, the most probable rupture force, F_{mp}, is linearly related to the logarithm of the pulling rate, r_F, as $F_{mp} = k_BT/x_\beta[\ln(r_F) - \ln(k_{off} \times k_BT/x_\beta)]$. Here, k_{off} is the dissociation rate of the unstressed bond, and x_β is the putative distance between the ground and transition states, k_B is Boltzmann's constant, and T is the absolute temperature ($T = 295$ K in these measurements). The determination of the number of bonds contributing to the histograms was achieved through a systematic evaluation of fits of histograms to probability functions for N_b independent uncorrelated, bonds (44) (Supporting Material). F-tests determined whether the inclusion of additional bonds in a model is statistically justified (45,46). Only models that best fit the data at all loading rates examined were selected. We also tested whether observations could be described by multivalent tip-surface contacts. The extensive series of tests and statistical criteria used to analyze measured force histograms are described in the Supporting Material.

RESULTS

SFA measurements

Force-distance profiles of W2A and CEC1–5 adhesion

To address the effect of the W2A mutation on C-cadherin adhesion, surface force measurements quantified the resulting

changes in the normalized force-distance curves (24). Using similar densities of CEC1–5-His$_6$ and W2A-His$_6$ ectodomains immobilized on the bilayers made it possible to directly compare force profiles and adhesion energies. The surface density of CEC1–5-His$_6$ was 1.4 ± 0.1 × $10^4/\mu m^2$ and that of W2A-His$_6$ was 1.7 ± 0.1 × $10^4/\mu m^2$.

Because this surface density differed slightly from those used in prior studies (24), we first measured the forces between CEC1–5-His$_6$ monolayers (Fig. 2 *A*). On approach, the onset of steric repulsion is at D < ~450 Å. The repulsion increased with decreasing separation. Upon separation from D < 240 Å, the proteins adhered at D = 252 ± 6 Å, with a normalized pull-off force of F_{po}/R = −2.0 ± 0.4 mN/m. However, when the surfaces were separated from 260 Å < D < 300 Å, they adhered farther out, at D = 314 ± 5 Å, with a pull-off force of F_{po}/R = −1.9 ± 0.3 mN/m. Finally, when the surfaces were separated from 320 Å < D < 390 Å, the cadherins bound at D = 402 ± 6 Å with a pull-off force of F_{po}/R = −0.7 ± 0.3 mN/m. We refer to these three bound states as the inner, middle, and outer bonds (24,26,38). These results are summarized in Table 1. Prior studies mapped the inner and outer bonds to EC3 and EC1, respectively, and showed that the middle bond requires EC3 and EC1 (26).

Use of domain deletion mutants maps regions required for cadherin binding

The force profiles between W2A-His$_6$ monolayers (Fig. 2 *B*) differed from those measured with wild-type ectodomains. First, during approach, the W2A ectodomains spontaneously jumped from ~400 Å to 273 ± 14 Å, where they briefly paused before finally coming to rest at the equilibrium separation of 226 ± 5 Å. Such jumps occur when the gradient of an attractive potential exceeds the spring constant (47).

The brief pause in the jump between 400 Å and 226 Å suggests the existence of an intervening barrier in the intersurface potential. Indeed, the W2A mutants adhered at two different membrane separations. The first bond, which is at this intermediate distance, failed at D = 311 ± 7 Å with a pull-off force of F/R = −1.0 ± 0.2 mN/m (Table 1). The second bond ruptured at D = 238 ± 6 Å, near the resting position, with a pull-off force of F_{po}/R = −1.6 ± 0.2 mN/m. The W2A mutants did not adhere at ~402 Å—the position of the putative EC1-EC1 bond (Fig. 2 *B*). This is similar to interactions between canine E-cadherin W2A mutants (17). Thus, we attribute adhesion at 400 Å to the W2-dependent EC1-EC1 bond (6,12).

Fig. 2 *C* shows the force-distance curves between W2A-His$_6$ and wild-type CEC1–5-His$_6$ monolayers. These proteins also spontaneously jumped in from ~400 Å, paused briefly near 300 Å, and then came to rest at the equilibrium separation of ~250 Å. Upon separation, the proteins adhered at the three membrane distances D = 252 ± 5 Å, 321 ± 5 Å, and 397 ± 9 Å with respective pull-off forces of −1.5 ± 0.4, −1.2 ± 0.2, and −0.6 ± 0.3 mN/m (Table 1). Fig. 3 compares the different estimated bond energies measured with the CEC1–5 and W2A mutant.

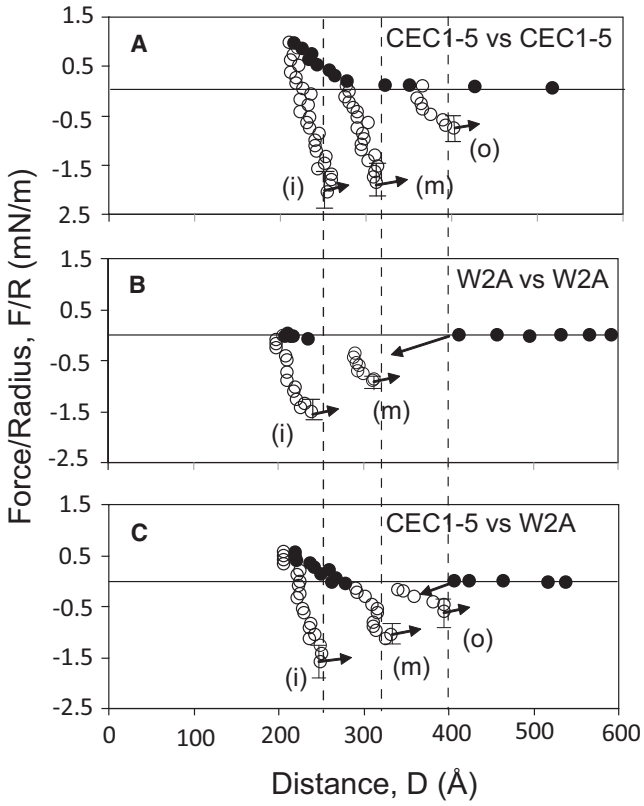

FIGURE 2 Normalized force-distance profiles between oriented monolayers of CEC1–5-His$_6$ and W2A-His$_6$. Solid circles indicate forces measured during approach, and open circles indicate forces measured during separation. (*A*) Normalized force-distance curves between oriented monolayers of CEC1–5-His$_6$. Right-pointing arrows indicate bond failure and jumps out of contact. Error bars represent the mean ± SD. Here, the inner bond is at 252 ± 6 Å (*i*), the middle bond at 314 ± 6 Å (*m*), and the outer bond at 402 ± 6 Å (*o*). Vertical dashed lines show the alignment of the three adhesive minima in the different measurements. (*B*) Normalized force-distance curves between oriented W2A-His$_6$ monolayers. Left-pointing arrows indicate jumps into contact. (*C*) Normalized force-distance curves measured between W2A and CEC1–5-His$_6$.

The adhesion between W2A-His$_6$ and CEC1–5-His$_6$ at 397 ± 9 Å indicates that EC1 domains can form half of a strand dimer. Within experimental error, the adhesion at 397 Å is comparable to that measured for EC1-EC1 bonds between wild-type proteins (p = 0.18). Adhesion at 321 ± 9 Å (middle bond) is statistically similar to adhesion between identical W2A mutants at 311 ± 7 Å. However, the adhesion at 252 ± 5 Å (inner bond) is 55% lower than between wild-type CEC1–5-His$_6$ monolayers (p < 0.01). The substantial adhesion attenuation suggests that the W2A mutation alters, but does not eliminate, bonds involving domains that are distal to the W2 binding site.

Measurements with CEC345-Fc mapped the inner bond to this segment of the ectodomain. The CEC345-Fc fragment

TABLE 1 Adhesion between protein pairs measured with the SFA

	Inner bond		Middle bond		Outer bond	
Protein pair	Adhesion (mN/m)	Complex length (Å)	Adhesion (mN/m)	Complex length (Å)	Adhesion (mN/m)	Complex length (Å)
WT/WT	−2.0 ± 0.4	252 ± 6	−1.9 ± 0.3	314 ± 5	−0.7 ± 0.3	402 ± 6
W2A/W2A	−1.6 ± 0.2	238 ± 6	−1.0 ± 0.2	311 ± 7	ND	
WT/W2A	−1.5 ± 0.4	252 ± 5	−1.2 ± 0.2	321 ± 4	−0.6 ± 0.3	397 ± 9
WT/EC345	−0.7 ± 0.2	240 ± 11	ND		ND	
W2A/EC345	−0.6 ± 0.1	238 ± 11	ND		ND	

WT, wild-type; ND, not detected.

($1.5 \pm 0.1 \times 10^4$ cadherin/μm^2) bound wild-type CEC1–5-His_6 ($1.4 \pm 0.1 \times 10^4$ cadherins/μm^2) at a single membrane distance of $D = 300 \pm 11$ Å with a pull off force of $F_{po}/R = -0.7 \pm 0.2$ mN/m (Table 1). Subtracting the thickness of the protein A and Fc-tag (15 + 45 Å) used to anchor CEC345-Fc indicates that the end-to-end length of the protein complex at pull off is $D = 300$ Å $- (15 + 45) = 240 \pm 11$ Å. This corresponds quantitatively to the position of the inner bond measured between identical W2A-His_6 fragments. Opposed CEC345-Fc and W2A-His_6 similarly adhered at $D = 298 \pm 11$ Å with a pull-off force of $F_{po}/R = -0.6 \pm 0.1$ mN/m. These results suggest that the bonds at ~252 Å formed by wild-type CEC1–5-His_6 and W2A-His_6 involve the same binding interface, and that W2A reduces the corresponding adhesion energy.

AFM measurements of single bond rupture

The SFA measurements show that the W2A mutation eliminates EC1-dependent adhesion between W2A mutants and attenuates distal interactions by the ectodomains. If the W2A mutation allosterically modulates distal functional domains, then it would alter the intrinsic biophysical properties of cadherin bonds. However, SFA measurements report the population averaged adhesion and cannot distinguish changes in the intrinsic bond properties from mutation-related changes in the specific activity (average activity/mg protein). In contrast, AFM measurements detect single bonds between active proteins, but inactive proteins do not influence the measurements. Here, single bond rupture measurements with wild-type CEC1–5-Fc, W2A-His_6, and different domain deletion fragments mapped cadherin adhesive interactions to different structural regions. These measurements quantified the influence both of different EC domains and of the W2A mutation on the intrinsic bond properties.

Comparison of CEC12 and CEC1–5 single bond rupture

The histogram of the rupture forces measured between CEC12 fragments shows one dominant peak and a smaller peak at lower force (Fig. 4 *A*), similar to previous reports (19,22). Plots of the most probable rupture forces, F_{mp}, defined by the peak maxima, versus the logarithm of the loading rate, r_F, were linear. Linear least-squares fits to the data (Fig. 4 *E*, *solid lines*) determined that the histogram is best described by two uncorrelated bonds ($N_b = 2$) with the best-fit dissociation rates and x_β values summarized in Table 2 (44). The solid lines in Fig. 4 *A* are the probability distributions for both bonds computed with the fitted parameters.

There are two differences between the force histograms of CEC12 and CEC1–5 fragments. First, although there are also two obvious peaks, the main peak at the higher rupture force measured for CEC1–5 is consistently much broader than that observed for CEC12 (Fig. 4 *B*). Second, the maximum of the second peak shifts to a higher rupture force than the main peak in Fig. 4 *A*. Model fits show that the high force peak in Fig. 4 *B* is too broad to ascribe to a single bound state (Fig. S1 in the Supporting Material). To determine whether this broad peak masks other binding events, as reported previously (19,22), the cumulative distribution of the force data was fit to models for N_b independent bonds (details in Supporting Material). F-tests confirmed that a three-state ($N_b = 3$) model best describes the bond statistics at all pulling rates (Fig. 4 *B* and

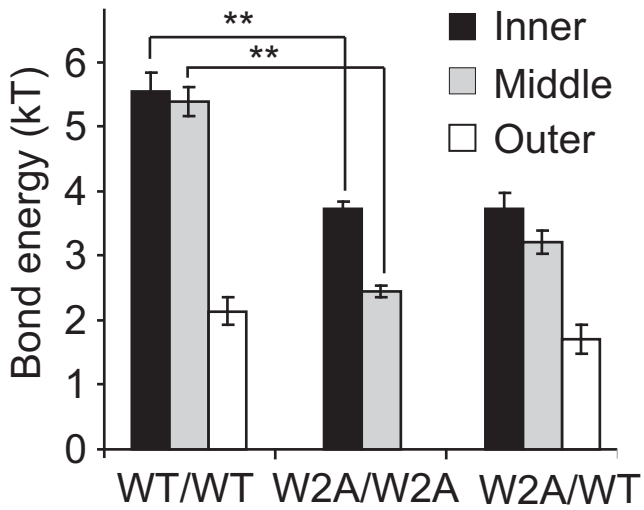

FIGURE 3 Estimated adhesion energies (in k_BT) for the inner, middle, and outer bonds for the cadherin interactions CEC1–5/CEC1–5, W2A/W2A, and CEC1–5/W2A. The bars are the means and error bars indicate the mean ± SD. $^{**}p < 0.01$ for the difference in adhesion energies between the inner and middle bonds of the W2A/W2A and CEC1–5/ CEC1–5 bonds.

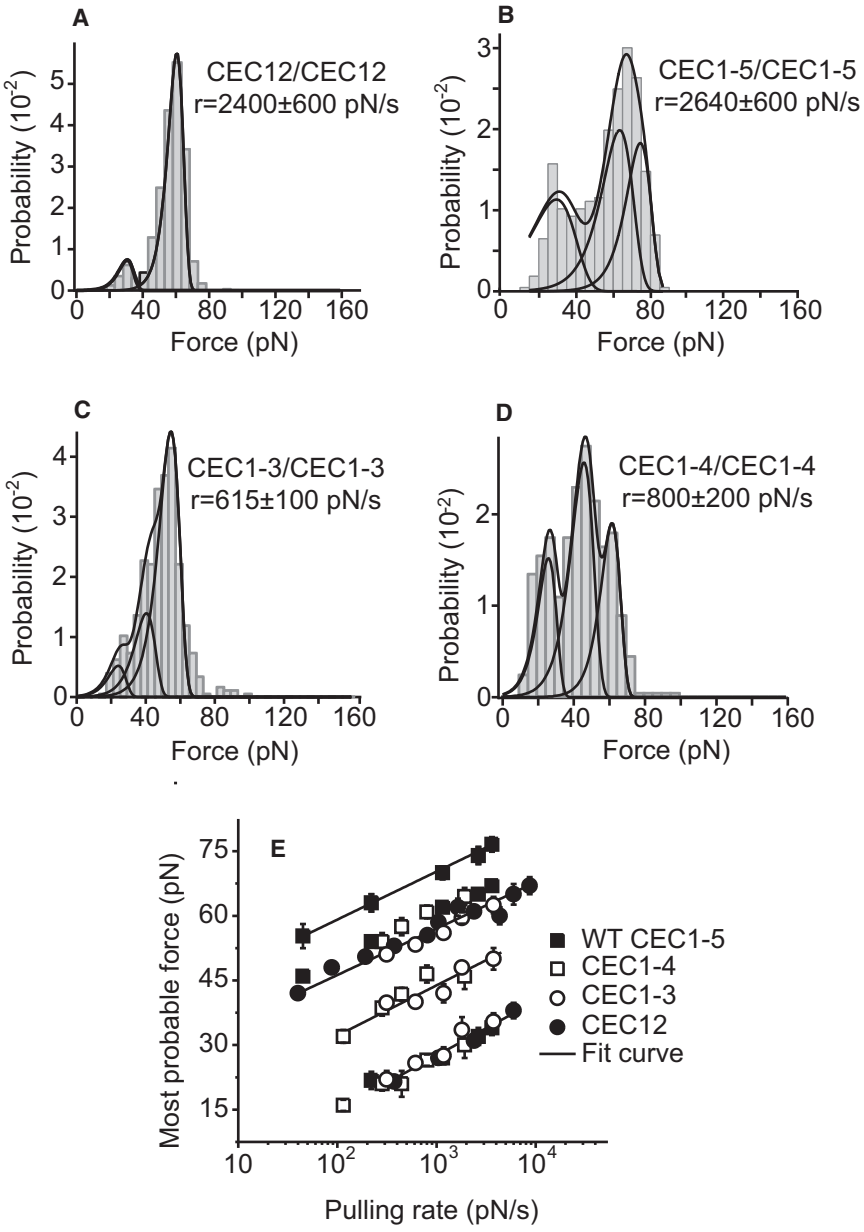

FIGURE 4 (*A–E*) Representative rupture force distributions between CEC12-Fc (*A*), CEC1–5-Fc (*B*), CEC1–3 (*C*), and CEC1–4 (*D*) fragments at the indicated pulling rates. (*E*) The most probable force, F_{mp}, of each bound state plotted against the logarithm of the pulling rate r_F. The solid lines are linear fits to the force spectra with best-fit parameters summarized in Table 2. Error bars smaller than the size of the symbols are not shown. Solid lines in *A–D* are probability distributions computed using the parameters obtained from the force spectra in *E*.

Table S1). Model tests also confirmed that the peak broadening is not due to multivalent tip-surface linkages (Supporting Material).

Fig. 4 *E* shows the force spectra of the most probable rupture force, F_{mp}, versus the logarithm of the pulling rate, r_F, for the three putative bonds underlying the distribution in Fig. 4 *B*. All three bonds exhibit linear force spectra, and least-squares analyses of the curves give the individual dissociation rates and x_β values (Table 2). The solid lines in Fig. 4 *B* are the probability distributions computed with the best-fit parameters. Note that the force spectra of the low-force and intermediate peak between CEC1–5-Fc fragments coincides with the two CEC12/CEC12 bonds (Fig. 4 *E*). However, the third bond is stronger (higher rupture force) than either of the two EC12-dependent bonds.

Interactions between CEC12-Fc and CEC1–5-Fc at several loading rates exhibit two bound states, with corresponding force spectra that overlap with those of the CEC12-Fc/CEC12-Fc bonds (Fig. S3 and Table 2). In contrast to the data in Fig. 4 *B*, these histograms are best described by a two-state model ($N_b = 2$).

Contribution of EC domains 3–5 to cadherin binding in AFM measurements

The measured rupture forces between identical 1), CEC1–3-Fc and 2), CEC1–4-Fc deletion mutants that lack EC45 and EC5, respectively, determined the contributions of domains EC4 and EC5 to single bond statistics. Fig. 4 *C* shows the force histogram measured with CEC1–3-Fc fragments at $r_F = 615 \pm 100$ pN/s. There is a prominent peak evident at

TABLE 2 Dissociation rates and x_β from linear fits to dynamic force spectra

	Weak		Intermediate		Strong	
Protein pair	k_{off} (s^{-1})	x_β (nm)	k_{off} (s^{-1})	x_β (nm)	k_{off} (s^{-1})	x_β (nm)
CEC12/CEC12	1.1 ± 0.4	0.74 ± 0.07	1.2 ± 0. 7 × 10^{-3}	0.86 ± 0.06	ND	ND
CEC12/CEC1245	0.8 ± 0.7	0.69 ± 0.14	2.5 ± 1 × 10^{-3}	0.88 ± 0.09	ND	ND
CEC1245/CEC1245	1.1 ± 0.4	0.68 ± 0.07	1.4 ± 1 × 10^{-3}	0.81 ± 0.07	ND	ND
CEC1245/CEC1–5	1.2 ± 1	0.6 ± 0.09	0.4 ± 0.2 × 10^{-3}	0.88 ± 0.07	ND	ND
CEC12/CEC1–5	1.0 ± 0.7	0.75 ± 0.07	0.8 ± 0.5 × 10^{-3}	0.9 ± 0.08	ND	ND
CEC1-3/CEC1–3	1.2 ± 0.8	0.71 ± 0.11	0.04 ± 0.035	0.79 ± 0.15	2 ± 1.5 × 10^{-3}	0.84 ± 0.07
CEC1-4/CEC1–4	1.1 ± 0.5	0.79 ± 0.09	0.02 ± 0.016	0.82 ± 0.17	2 ± 1 × 10^{-3}	0.75 ± 0.08
CEC1-5/CEC1–5	0.4 ± 0.3*	0.94 ± 0.12	0.5 ± 0.4 × 10^{-3}	0.86 ± 0.1	6 ± 3 × 10^{-5}	0.88 ± 0.08
CEC345/CEC345*	1.6 ± 0.9	0.79 ± 0.08	ND	ND	ND	ND
CEC345/CEC1–5*	0.8 ± 0.3	0.74 ± 0.06	ND	ND	ND	ND
W2A/W2A	1.4 ± 0.4	0.61 ± 0.12	ND	ND	ND	ND
W2A/CEC1–5*	1.3 ± 0.4	0.75 ± 0.07	0.02 ± 0.01	0.83 ± 0.08	ND	ND
W2A/CEC12*	0.8 ± 0.5	0.7 ± 0.09	0.02 ± 0.015	0.88 ± 0.09	ND	ND
W2A/CEC345	1.5 ± 0.3	0.58 ± 0.03	ND	ND	ND	ND

ND, not detected.
*See Supporting Material.

all pulling rates. Fits of the cumulative distribution to N_b-state models and the use of F-tests identified a low-force peak and an intermediate state (Fig. 4 *C* and Table 2). The intermediate peak was more prominent at lower pulling rates (Fig. S2) and has no counterpart in the CEC12/CEC12 histograms (see Fig. 4 *A* and Table 2). Force histograms measured between CEC1–4-Fc fragments exhibited three distinct peaks at all pulling speeds (Fig. 4 *D*), with the bond parameters summarized in Table 2. Thus, fragments containing the first three EC domains form three bonds (Fig. 4, *B–D*). These three bonds include the same two EC12-dependent bonds, in addition to a third bound state. Comparison with the histogram in Fig. 4 *B* suggests that the strength and formation frequency of the third bound state increase with the successive addition of domains EC4 and EC5, and that the latter two domains stabilize this additional interaction.

AFM measurements with the C-cadherin deletion mutant CEC1245-Fc tested the impact of EC3 on cadherin binding. Force histograms and force spectra for binding between CEC1245 and 1), CEC1–5, 2), CEC1245, or 3), CEC12 were determined. In all three cases, fits of the cumulative distributions to probability distributions for N_b independent bonds, together with F-test models, showed that the data are all best described by two ($N_b = 2$) distinct binding states. The force spectra are tightly clustered within ±5 pN of the force spectra for the two CEC12/CEC12 bonds. The CEC1245/CEC1–5 bonds are slightly stronger than EC12/EC12 bonds, but they are statistically weaker than the third, strongest, bond measured between CEC1–5 fragments.

W2A mutants alter the intrinsic properties of all cadherin bonds

The tryptophan at position 2 is required for cadherin function. Surface force measurements show that W2A mutants do, however, retain weak binding (Fig. 2). AFM measurements of W2A/W2A interactions at several pulling rates also exhibit a single, narrow peak (Fig. S4 *B*) corresponding to a bond with $k_{off} = 1.4 \pm 0.4\ s^{-1}$ and $x_\beta = 0.61 \pm 0.05$ nm.

Comparison of bond rupture between 1), W2A and CEC345-Fc and 2), between wild-type CEC1–5-Fc and CEC345-Fc was made to map this W2A/W2A bond to different cadherin segments, analogous to the SFA measurements (Table 1). Measurements between W2A and EC345-Fc tested the hypothesis that the W2A/W2A bond involves EC3–5, as suggested by the intermembrane distance at which these same fragments bind in SFA measurements (Table 1). The force histogram for the W2A/CEC345 interaction exhibits a single peak (Fig. S5), which corresponds to a single bond with $k_{off} = 1.5 \pm 0.3\ s^{-1}$ and $x_\beta = 0.58 \pm 0.03$ nm (Table 2). The latter values are statistically the same as those measured between identical W2A mutants ($p = 0.57$), suggesting that both bonds are due to the same interaction. By analogy with the SFA findings that the inner bond between W2A monolayers and between W2A and CEC345-Fc are at the same end-to-end complex distance (Table 1), we postulate that the peaks in Fig. S4 require EC3.

DISCUSSION

The measured interactions between different cadherin mutants determined with both AFM and SFA demonstrate that the distinct force signatures observed using these experimental approaches are linked to the distinct biochemical properties of the proteins examined. Four main conclusions emerge from these findings. First, both approaches show that the cadherin ectodomains form multiple, independent bonds that involve EC1 and at least one additional domain distal to the N-terminal region. Second, both experimental measurements confirm that one of these bonds is due to the W2 strand exchange, and that W2A alters the intrinsic properties of the

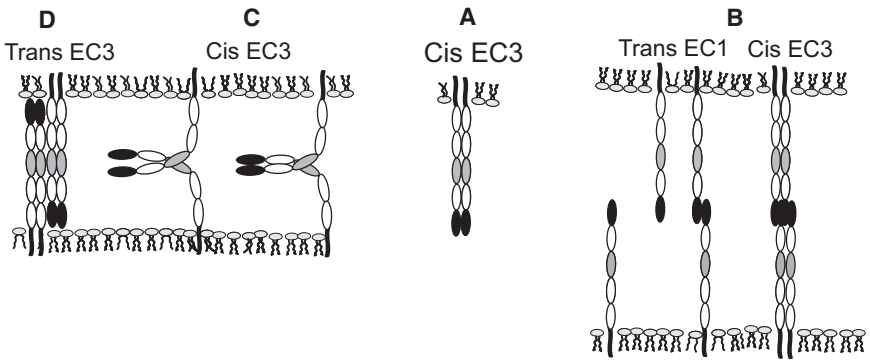

FIGURE 5 Models of cadherin binding consistent with the data. (*A*) *Cis* (lateral dimers) stabilized by an EC3-dependent bond (*gray domain*). (*B*) The formation of *trans* (adhesive) dimers between EC1 domains on opposing proteins could lead to the accumulation of cadherins locally to promote the formation of *cis* dimers through EC3-dependent bonds (*gray domains*). (*C*) In force measurements, and possibly on the cell surface, *cis* bonds (*gray*) can also form between cadherins on opposing probe surfaces. The force measurements would sample adhesive states due to both lateral and adhesive dimers. (*D*) Proteins form antiparallel adhesive bonds stabilized by interactions between EC3 domains.

other cadherin bonds. Third, both confirm that the W2A mutants retain residual binding function, which appears to map to domains EC3–5. Finally, measurements with CEC1–3, CEC1–4, and CEC1–5 suggest that EC4 and EC5 stabilize or augment the EC1-independent bound state, in agreement with prior SFA measurements of these same fragments (26).

Although these findings parallel those of earlier reports, this study compares extensive structure/function analyses of single bond rupture measurements with SFA measurements with the same proteins. The results document cross talk between cadherin extracellular domains that modulates the different cadherin binding interactions. They also provide quantitative evidence for allosteric cross talk between the W2 binding pocket and distal functional domains in the extracellular region. In contrast to previous studies, we use the two independent complementary methods here to inform or corroborate analyses of results obtained with each approach.

Force histograms obtained with cadherin fragments containing EC12 but not EC3 all exhibit two bound states. The colinearity of the force spectra of both EC12-dependent bonds measured with several different cadherin fragments (Fig. 4 *E*) suggests a common binding interface. Differences in the parameters (Table 2) are attributed to standard error in experimentally determined slopes and intercepts used to extract bond parameters (Supporting Material).

The addition of domains 3–5 coincides with the emergence of a third bound state in force histograms. With CEC1–5, the third bond, evident from peak broadening and a shift in the force maximum of the second prominent peak is supported by analyses of cumulative distributions and the use of F-tests to compare models. Both the strength and formation frequency of this additional adhesive state depend on domains EC4 and EC5. Although this bond requires EC3, removing EC5 also decreased its strength and increased its dissociation rate. The amplitude of a third peak is clearly visible in histograms of CEC1–4/CEC1–4 rupture forces, but loss of EC4 and EC5 reduces the amplitude (frequency). It is important to note that this third bond cannot be explained by multivalent tip-surface contact. The dependence of the properties of this third state on EC4 and EC5 parallels the attenuation of the inner bond in SFA measurements, after EC4 and EC5 deletion (26). We therefore speculate that the third peak observed in single bond rupture measurements is the EC3-dependent inner bond in SFA force-distance profiles. AFM and SFA results thus suggest that thermodynamic coupling between domains EC3–5 governs the strength of this bond.

Multiple peaks in force histograms measured by AFM could rise from multivalent tip-surface bonds (48) or from multiple, independent bound states between single cadherins (19,22). The detailed and extensive analyses of the histograms, the link between histogram features and the biochemical identity of the protein fragment used, and supporting data from SFA measurements rule out multivalent tip-surface bonds as the cause of the differences in the force signatures. A model in which multiple cadherin segments contribute to binding agrees with SFA results described here and previously (26), and with previous single bond rupture studies of mouse E-cadherin and *Xenopus* C-cadherin (19,22).

It is important to point out that the rotational flexibility of cadherins tethered to polymers in the AFM measurements and structural flexibility of the cadherin extracellular domain (24,33,49) precludes the unambiguous assignment of adhesive interactions measured by AFM or SFA to either *cis* or *trans* bonds. Recent fluorescence resonance energy transfer studies (50) and electron tomography images (49,51) suggest that the additional binding states may not correspond to antiparallel adhesive bonds. However, there is increasing evidence that cadherin oligomerization is required for its adhesive function (11,14,52–55), and several reports show that reconstitution of the binding properties of the full-length extracellular domain requires multiple domains (19–22, 24–26). Different oligomerization sites have been proposed (11,12,53), including calcium bridging between E-cadherin EC12 fragments (56). To date, no structure-based models account for all of the experimental findings. Nevertheless, this study and prior results both support the EC12/EC12 strand exchange model and further document the existence of other cadherin interactions that involve EC domains distal to the W2 docking site (Fig. 5).

W2A eliminates EC1-dependent binding in both AFM and SFA measurements, consistent with the strand exchange model (6,12,17). In SFA measurements, opposing W2A

monolayers also rapidly and spontaneously jump into contact at 226 Å, signifying the loss of outer barriers (adhesive traps), which otherwise impede this movement (21). Additional effects of the W2A mutation on force histograms and on force-distance profiles also suggest that W2 docking in the hydrophobic pocket allosterically regulates distal cadherin interactions. In SFA measurements, the W2A mutant binds CEC1–5 at the same three distances as between identical CEC1–5 fragments, but the mutation reduces the inner and middle bond strengths. This agrees with the behavior of the E-cadherin W2A mutant (26). The attenuation of additional (lateral) binding interactions would also account for the W2A-dependent encryption of a dimer-specific epitope and concomitant exposure of a monomer-specific epitope near EC4 of C-cadherin (32).

In AFM measurements, opposing W2A mutants form a single bond with a fast dissociation rate. This weak bond is not attributable solely to EC12/EC12 binding, as proposed elsewhere (16), because W2A also binds CEC3–5. The W2A/W2A peak could embed both the weak EC12/EC12 and EC345/EC345 bonds, which have very similar strengths and dissociation rates (Table 2).

In conclusion, both SFA and AFM measurements demonstrate thermodynamic coupling between C-cadherin EC domains. These results support a model in which W2 docking globally regulates cadherin interactions, including possible lateral interactions that do not directly involve EC1. This postulated long-range interdomain cross talk is supported by several independent findings, namely, 1), the exposure of monomer-specific epitopes near EC4 and EC5 in the W2A mutant of C-cadherin; 2), the effect of W2 docking on the exposure of a distal epitope in the EC1 domain; and 3), the loss of EC1/EC1 adhesion after mutation of the calcium-binding site at the EC2/EC3 junction (D216A) (16,17,32). Such allosteric regulation could reconcile the importance of W2 with additional cadherin interactions (13,16,18). These findings suggest a more comprehensive model for cadherin-mediated cell adhesion in which multiple domains contribute to lateral and adhesive bonds. Because of the similar behavior exhibited by several Type I classic cadherins, including C-cadherin, mouse E-cadherin, canine E-cadherin, chicken N-cadherin, and human N-cadherin (19,21,22,24,25,38,40), it is reasonable to speculate that this is characteristic of Type I cadherins. Whether such behavior extends to other cadherins, such as Type II or desmosomal cadherins, for example, remains to be determined.

SUPPORTING MATERIAL

Six figures and one table are available at http://www.biophysj.org/biophysj/supplemental/S0006-3495(10)00429-7.

This work was supported by the National Science Foundation, Chemical, Bioengineering, Environmental, and Transport Systems Division (grant 0853705).

REFERENCES

1. Takeichi, M. 1995. Morphogenetic roles of classic cadherins. *Curr. Opin. Cell Biol.* 7:619–627.
2. Gumbiner, B. M. 2005. Regulation of cadherin-mediated adhesion in morphogenesis. *Nat. Rev. Mol. Cell Biol.* 6:622–634.
3. Cavallaro, U., and G. Christofori. 2004. Cell adhesion and signalling by cadherins and Ig-CAMs in cancer. *Nat. Rev. Cancer.* 4:118–132.
4. Kitagawa, M., M. Natori, …, S. T. Suzuki. 2000. Mutation analysis of cadherin-4 reveals amino acid residues of EC1 important for the structure and function. *Biochem. Biophys. Res. Commun.* 271:358–363.
5. Tamura, K., W. S. Shan, …, L. Shapiro. 1998. Structure-function analysis of cell adhesion by neural (N-) cadherin. *Neuron.* 20:1153–1163.
6. Häussinger, D., T. Ahrens, …, S. Grzesiek. 2004. Proteolytic E-cadherin activation followed by solution NMR and x-ray crystallography. *EMBO J.* 23:1699–1708.
7. Pertz, O., D. Bozic, …, J. Engel. 1999. A new crystal structure, Ca^{2+} dependence and mutational analysis reveal molecular details of E-cadherin homoassociation. *EMBO J.* 18:1738–1747.
8. Chitaev, N. A., and S. M. Troyanovsky. 1998. Adhesive but not lateral E-cadherin complexes require calcium and catenins for their formation. *J. Cell Biol.* 142:837–846.
9. Shan, W. S., H. Tanaka, …, L. Shapiro. 2000. Functional *cis*-heterodimers of N- and R-cadherins. *J. Cell Biol.* 148:579–590.
10. Harrison, O. J., E. M. Corps, and P. J. Kilshaw. 2005. Cadherin adhesion depends on a salt bridge at the N-terminus. *J. Cell Sci.* 118:4123–4130.
11. Troyanovsky, R. B., E. Sokolov, and S. M. Troyanovsky. 2003. Adhesive and lateral E-cadherin dimers are mediated by the same interface. *Mol. Cell. Biol.* 23:7965–7972.
12. Boggon, T. J., J. Murray, …, L. Shapiro. 2002. C-cadherin ectodomain structure and implications for cell adhesion mechanisms. *Science.* 296:1308–1313.
13. Koch, A. W., K. L. Manzur, and W. Shan. 2004. Structure-based models of cadherin-mediated cell adhesion: the evolution continues. *Cell. Mol. Life Sci.* 61:1884–1895.
14. Yap, A. S., W. M. Brieher, …, B. M. Gumbiner. 1997. Lateral clustering of the adhesive ectodomain: a fundamental determinant of cadherin function. *Curr. Biol.* 7:308–315.
15. Ozawa, M. 2002. Lateral dimerization of the E-cadherin extracellular domain is necessary but not sufficient for adhesive activity. *J. Biol. Chem.* 277:19600–19608.
16. Harrison, O. J., E. M. Corps, …, P. J. Kilshaw. 2005. The mechanism of cell adhesion by classical cadherins: the role of domain 1. *J. Cell Sci.* 118:711–721.
17. Prakasam, A., Y. H. Chien, …, D. E. Leckband. 2006. Calcium site mutations in cadherin: impact on adhesion and evidence of cooperativity. *Biochemistry.* 45:6930–6939.
18. Leckband, D., and A. Prakasam. 2006. Mechanism and dynamics of cadherin adhesion. *Annu. Rev. Biomed. Eng.* 8:259–287.
19. Bayas, M. V., A. Leung, …, D. Leckband. 2006. Lifetime measurements reveal kinetic differences between homophilic cadherin bonds. *Biophys. J.* 90:1385–1395.
20. Chappuis-Flament, S., E. Wong, …, B. M. Gumbiner. 2001. Multiple cadherin extracellular repeats mediate homophilic binding and adhesion. *J. Cell Biol.* 154:231–243.
21. Chien, Y. H., N. Jiang, …, D. Leckband. 2008. Two stage cadherin kinetics require multiple extracellular domains but not the cytoplasmic region. *J. Biol. Chem.* 283:1848–1856.
22. Perret, E., A. Leung, …, E. Evans. 2004. *Trans*-bonded pairs of E-cadherin exhibit a remarkable hierarchy of mechanical strengths. *Proc. Natl. Acad. Sci. USA.* 101:16472–16477.
23. Shan, W., Y. Yagita, …, D. R. Colman. 2004. The minimal essential unit for cadherin-mediated intercellular adhesion comprises extracellular domains 1 and 2. *J. Biol. Chem.* 279:55914–55923.

24. Sivasankar, S., B. Gumbiner, and D. Leckband. 2001. Direct measurements of multiple adhesive alignments and unbinding trajectories between cadherin extracellular domains. *Biophys. J.* 80:1758–1768.

25. Tsukasaki, Y., K. Kitamura, …, T. Yanagida. 2007. Role of multiple bonds between the single cell adhesion molecules, nectin and cadherin, revealed by high sensitive force measurements. *J. Mol. Biol.* 367: 996–1006.

26. Zhu, B., S. Chappuis-Flament, …, D. Leckband. 2003. Functional analysis of the structural basis of homophilic cadherin adhesion. *Biophys. J.* 84:4033–4042.

27. Ozawa, M., J. Engel, and R. Kemler. 1990. Single amino acid substitutions in one Ca^{2+} binding site of uvomorulin abolish the adhesive function. *Cell.* 63:1033–1038.

28. Handschuh, G., S. Candidus, …, K. F. Becker. 1999. Tumour-associated E-cadherin mutations alter cellular morphology, decrease cellular adhesion and increase cellular motility. *Oncogene.* 18:4301–4312.

29. Handschuh, G., B. Luber, …, K. F. Becker. 2001. Single amino acid substitutions in conserved extracellular domains of E-cadherin differ in their functional consequences. *J. Mol. Biol.* 314:445–454.

30. Swain, J. F., and L. M. Gierasch. 2006. The changing landscape of protein allostery. *Curr. Opin. Struct. Biol.* 16:102–108.

31. Hynes, R. O. 2002. Integrins: bidirectional, allosteric signaling machines. *Cell.* 110:673–687.

32. Tsuiji, H., L. Xu, …, B. M. Gumbiner. 2007. Cadherin conformations associated with dimerization and adhesion. *J. Biol. Chem.* 282:12871–12882.

33. Sotomayor, M., and K. Schulten. 2008. The allosteric role of the Ca^{2+} switch in adhesion and elasticity of C-cadherin. *Biophys. J.* 94: 4621–4633.

34. Schuck, P. 1997. Use of surface plasmon resonance to probe the equilibrium and dynamic aspects of interactions between biological macromolecules. *Annu. Rev. Biophys. Biomol. Struct.* 26:541–566.

35. Leckband, D. 1995. The surface apparatus—a tool for probing molecular protein interactions. *Nature.* 376:617–618.

36. Israelachvili, J. N. 1973. Thin film studies using multiple-beam interferometry. *J. Colloid Interface Sci.* 44:259–272.

37. Israelachvili, J. N. 1992. Intermolecular and Surface Forces, 2nd ed. Academic Press, New York.

38. Prakasam, A. K., V. Maruthamuthu, and D. E. Leckband. 2006. Similarities between heterophilic and homophilic cadherin adhesion. *Proc. Natl. Acad. Sci. USA.* 103:15434–15439.

39. Leckband, D., W. Müller, …, H. Ringsdorf. 1995. Molecular mechanisms determining the strength of receptor-mediated intermembrane adhesion. *Biophys. J.* 69:1162–1169.

40. Shi, Q., Y. H. Chien, and D. Leckband. 2008. Biophysical properties of cadherin bonds do not predict cell sorting. *J. Biol. Chem.* 283: 28454–28463.

41. Wieland, J. A., A. A. Gewirth, and D. E. Leckband. 2005. Single molecule adhesion measurements reveal two homophilic neural cell adhesion molecule bonds with mechanically distinct properties. *J. Biol. Chem.* 280:41037–41046.

42. Hutter, J. L., and J. Bechhoefer. 1993. Calibration of atomic-force microscope tips. *Rev. Sci. Instrum.* 64:1868–1873.

43. Merkel, R., P. Nassoy, …, E. Evans. 1999. Energy landscapes of receptor-ligand bonds explored with dynamic force spectroscopy. *Nature.* 397:50–53.

44. Evans, E., and K. Ritchie. 1997. Dynamic strength of molecular adhesion bonds. *Biophys. J.* 72:1541–1555.

45. Beck, J. V., and K. J. Arnold. 1977. Parameter Estimation in Engineering and Science. Wiley, New York.

46. Hukkanen, E. J., J. A. Wieland, …, R. D. Braatz. 2005. Multiple-bond kinetics from single-molecule pulling experiments: evidence for multiple NCAM bonds. *Biophys. J.* 89:3434–3445.

47. Marra, J., and J. Israelachvili. 1985. Direct measurements of forces between phosphatidylcholine and phosphatidylethanolamine bilayers in aqueous electrolyte solutions. *Biochemistry.* 24:4608–4618.

48. Baumgartner, W., P. Hinterdorfer, …, D. Drenckhahn. 2000. Cadherin interaction probed by atomic force microscopy. *Proc. Natl. Acad. Sci. USA.* 97:4005–4010.

49. Pokutta, S., K. Herrenknecht, …, J. Engel. 1994. Conformational changes of the recombinant extracellular domain of E-cadherin upon calcium binding. *Eur. J. Biochem.* 223:1019–1026.

50. Zhang, Y., S. Sivasankar, …, S. Chu. 2009. Resolving cadherin interactions and binding cooperativity at the single-molecule level. *Proc. Natl. Acad. Sci. USA.* 106:109–114.

51. Lambert, O., J. C. Taveau, …, A. Brisson. 2005. The basic framework of VE-cadherin junctions revealed by cryo-EM. *J. Mol. Biol.* 346:1193–1196.

52. Bibert, S., H. Ayari, …, D. Gulino-Debrac. 2008. Establishment of cell-cell junctions depends on the oligomeric states of VE-cadherin. *J Biochem.* 143:821–832.

53. Bibert, S., M. Jaquinod, …, D. Gulino-Debrac. 2002. Synergy between extracellular modules of vascular endothelial cadherin promotes homotypic hexameric interactions. *J. Biol. Chem.* 277:12790–12801.

54. Brieher, W. M., A. S. Yap, and B. M. Gumbiner. 1996. Lateral dimerization is required for the homophilic binding activity of C-cadherin. *J. Cell Biol.* 135:487–496.

55. Takeda, H., Y. Shimoyama, …, S. Hirohashi. 1999. E-cadherin functions as a *cis*-dimer at the cell-cell adhesive interface in vivo. *Nat. Struct. Biol.* 6:310–312.

56. Nagar, B., M. Overduin, …, J. M. Rini. 1996. Structural basis of calcium-induced E-cadherin rigidification and dimerization. *Nature.* 380:360–364.